Inhibiting Asphaltene Deposition Using Polymer Functionalized Nanoparticles in Microfluidic Porous Media

Thao Vy Nguyen,[†] Zhuqing Zhang,[†] Jianxin Wang,[‡] Aparna Sagi,[¶] Yogesh Kapoor,[§] Tanguy Terlier,[‖] and Sibani Lisa Biswal[*,†]

[†]*Department of Chemical and Biomolecular Engineering, Rice University, Houston, Texas 77005, United States*

[‡]*Chevron Corporation, Houston, Texas 77002, United States*

[¶]*Shell Technology Center, Houston, Texas 77082, United States*

[§]*Occidental Corporation, Houston, Texas 77046, United States*

[‖]*SIMS Laboratory, Shared Equipment Authority, Rice University, Houston, Texas 77005, United States*

E-mail: biswal@rice.edu

Abstract

Asphaltenes are the heaviest and most polarizable fraction of crude oil. During the oil production process, changes in temperature, pressure, and oil composition can destabilize asphaltenes. This destabilization leads to asphaltene aggregation and deposition, which can cause major clogging problems both in the wellbore and near-wellbore regions as well as the production facilities. In this study, we developed and investigated the application of AA-AMPS-functionalized magnetic nanoparticles as a surface coating in inhibiting asphaltene deposition. The use of the porous media microfluidic platform allows for the efficient evaluation of the effectiveness of the nanoparticle coating

in mitigating asphaltene deposition in various crude oils. We demonstrated that the nanoparticle coating is effective in inhibiting asphaltene deposition, showing up to 75% improvement in permeability change. The study also explores the dynamics of asphaltene aggregation and deposition in different crude oils. We identified factors such as asphaltene aggregate size as well as the aggregates' physical and chemical characteristics that can determine the effectiveness of different mitigation methods.

Introduction

Asphaltenes constitute the heaviest and the most polarizable component of crude oil.[1] They are usually referred to as the "cholesterol of petroleum" because of their tendency to aggregate and precipitate, causing clogging problems not only in the wellbore and near-wellbore regions, but also in pipelines and production facilities.[2,3] During the oil production process, changes in temperature, pressure, and composition can destabilize asphaltenes, leading to the formation of asphaltene nano- and micro-aggregates.[4,5] These aggregates can cause flow assurance issues by plugging small pore throats via mechanical trapping or depositing on rock surfaces through surface interaction and adsorption.[6,7] This leads to significant permeability reduction in porous media, resulting in production loss and serious formation damage. Asphaltene remediation procedures can cause unnecessary production shutdowns that can cost up to several millions of dollars in economic impact.[2]

Asphaltenes have been an active research area within the last few decades, both in industry and academia. Common solutions used to tackle this problem include mechanical removal, solvent soaking, or the use of asphaltene chemical inhibitors. These methods, however, carry certain limitations. The use of mechanical removal can be very limited in the geometry of the applicable surface, while solvent soaking involves the use of aromatic solvents (benzene, toluene, ethylbenzene, and xylene) that are toxic, environmentally unfriendly, and costly. Lastly, the effectiveness of asphaltene chemical inhibitors depends on the crude oil's chemical composition, which can be highly variable.[8–11] No single chemical

inhibitor is universally effective across all types of crude oils. Consequently, it is imperative to seek innovative and more potent approaches to address the challenge of asphaltene deposition.

In this study, we investigated the effectiveness of polymer-functionalized nanoparticles on asphaltene mitigation through surface coating. By taking advantage of the electrostatic forces governing the adsorption mechanisms, we introduce negatively-charged polymer-functionalized magnetic nanoparticles that chemically adsorb onto the mineral surface. The poly-electrolyte copolymers of acrylic acid and 2-acrylanmido-2-methylpropanesufolnic acid (AA-AMPS) functionalized on the surface of the nanoparticles not only help stabilize the nanoparticle colloidal suspension,[12] but also provide electrostatic and steric repulsions that help prevent asphaltenes from depositing onto the nanoparticle-coated surface.

We approach this study using the microfluidic platform. Recently, microfluidics has been gaining attention as an efficient screening platform that can produce a large amount of data using minimal materials in a short span of time.[13] With advanced visualization tools, microfluidics allows the monitoring of in-situ processes in real-time, providing insights into the working mechanisms behind processes in the porous media that were challenging to study before.[10,14–19]

There are many studies on the behavior of asphaltenes in a model oil system, where asphaltenes were fractionated from crude oil and redissolved into a solvent (toluene). This approach ignores the effects of the components in crude oil, specifically resins, which have been shown to have an effect on the stability of asphaltenes.[20–23] This study delved into various crude oil systems, encompassing samples gathered from diverse sources, with each exhibiting distinct and contrasting physical and chemical attributes. This allows us to study the aggregation and deposition behaviors of asphaltenes under the influence of the other components in the crude oil, which are more representative of the processes happening within the reservoir. While studies involving crude oil can be limited due to the opaque nature of the liquid, microfluidic technology allows for the continuous monitoring of the processes, giving

better insights into the dynamics of the asphaltene deposition process. Furthermore, it has been demonstrated that the high asphaltene content in the oil is not necessarily associated with the high risk of asphaltene precipitation and deposition; on the contrary, relatively light oils with low asphaltene content are more likely to undergo asphaltene aggregation and precipitation.[24] Due to the complex nature of crude oil and asphaltenes in particular, there has not been an asphaltene mitigation method universally effective for all oil sources. The diversification in crude oil samples we had in this study would give us a better understanding as well as an accurate evaluation of our asphaltene mitigation method. This article studies the effectiveness of AA-AMPS-functionalized magnetic nanoparticles in asphaltene mitigation through surface coating in a microfluidic porous media. To the best of our knowledge, these functionalized nanoparticles have not been previously explored in asphaltene mitigation in crude oil systems.

Materials and Methods

Materials

Deionized (DI) water with a reistivity of 18.2 MΩ.cm was obtained from a Barnstead Nanopure water purification system (Thermo Scientific). Iron chloride tetrahydate, iron chloride hexehydrate, citric acid monohydrate, amonium hydroxyde (28-30%), (3-aminopropyl) triethoxysilane (APTES), and n-heptane were purchased from Sigma-Aldrich. Glacial acetic acid, sodium hydroxyde (1N), hydrochloric acid acid (1N), sodium chloride, 1-ethyl-3-(3-dimethylaminopropyl) carbodiimide (EDC), and toluene were purchased from Fischer Scientific. Acrylic acid and 2-acrylanmido-2-methylpropanesufolnic acid (AA-AMPS, 1:1) copolymer solution (100KDa) was obtained from SNF Holding Company. The four crude oils used in this study are from the Gulf of Mexico, with properties listed in Table 1.

Table 1: Properties of Crude Oils at 1 atm and 20^{o}C

Properties	Crude A	Crude B	Crude C	Crude D
Density @ 20^{o}C (g/cm^3)	0.850	0.880	0.892	0.902
Viscosity @ 20^{o}C (cP)	5.6	19.0	47.7	57.5
Saturates (wt %)	44.1	57.4	37.5	34.9
Aromatics (wt %)	44.5	19.2	35.6	33.4
Resins (wt %)	9.1	18.3	15.2	13.8
Asphaltenes (wt %)	2.3	5.1	11.7	17.9

Synsthesis of Polymer-Functionalized Magnetic Nanoparticles

1. Synthesis of Iron Oxide Magnetic Nanoparticles (MNPs)

The synthesis of magnetic nanoparticles followed a previously established procesdure.[12,25–28] Briefly, 2.15 g of iron chloride tetrahydrate and 5.875 g of iron chloride hexahydrate were dissolved in 100 mL of DI water. 0.125 g of citric acid monohydrate was added to the solution. The solution was then heated up to 90^{o}C with vigorous stirring. 24.2 mL of ammonium hydroxide (28%) was added into the solution to establish an alkaline condition for the initiation of MNPs, and the reaction was continued for 2 hours at 90^{o}C. The reaction solution was then cooled down to room temperature, and the MNPs were collected from the solution using magnetic separation. MNPs were washed 3 times using DI water, and between each washing step, probe-sonication was applied to facilitate the dispersion of NMPs. After the last washing step, MNPs were re-dispersed in DI water to make the final volume of 50 mL (concentration of 50 mg MNPs/mL).

2. Synthesis of Amine-Functionalized Magnetic Nanoparticles (NH_2-MNPs)

The functionalization of amine on MNPs was achieved through the APTES coating process,[26–28] such that 2.96 mL of APTES and 1.34 mL of glacial acetic acid were added into 28 mL of DI water at room temperature. The hydrolysis was carried out for 1 hour under acidic condition, then the pH of the solution was adjusted to 8 by adding 1N sodium hydroxide solution. 10 mL of MNPs (concentration of 50 mg MNPs/mL) was then ultra-sonicated and added drop-wise into the APTES solution. DI water was added such that the final reaction

volume is 100 mL. The coating reaction was then carried out at 65^{o}C for 24 hours, after which the reaction solution was cooled down to room temperature, where NH_2-MNPs were collected by magnetic separation and washed 3 times with DI water with probe-sonication between each washing step. NH_2-MNPs were then re-dispersed in DI water to make the final volume of 10 mL (concentration of 50 mg NH_2-MNPs/mL). The pH of the solution was adjusted to 4.5 by adding 1N hydrochloric acid solution to maintain the stability of the nanoparticles.

3. Synthesis of AA-AMPS-Functionalized Magnetic Nanoparticles (AA-AMPS-MNPs)

The functionalization of AA-AMPS on NH_2-MNPs followed the procedures previously established by Xue et al with some minor modifications.[12] 1.94 g of AA-AMPS copolymer was dissolved in 10 mL of DI water. The pH of the solution was adjusted to 4.7 using 1N hydrochloric acid solution. The copolymer was then activated with 1.08 mg of EDC for 10 minutes at room temperature. 2 mL of probe-sonicated NH_2-MNPs were then added drop-wise into the copolymer solution, and the reaction was continued for 5 minutes under probe-sonication. 30% sodium chloride solution was then added to the solution to obtain 3% salinity. The pH of the reaction solution was adjusted to 4.7, and the reaction was continued for 24 hours at room temperature. After this, the AA-AMPS-MNPs were collected and washed 3 times before being re-dispersed into DI water, making the final solution volume 10 mL with a concentration of 10 mg AA-AMPS-MNPs/mL.

Characterization of Polymer-Functionalized Magnetic Nanoparticles

Fourier transform infrared spectroscopy (FTIR) was used to characterize the surface chemical composition of the nanoparticles. FTIR was performed using the Thermo Scientific Nicolet iS50 FT-IR spectrometer and Smart iTR with a diamond window (Thermo Scientific). The samples were dried, powdered, and placed on the diamond window of the Smart iRT, and the spectra were recorded with wavelengths between 450 cm^{-1} and 4000

cm^{-1}.

The size of the nanoparticles was measured in DI water, and the zeta potential of the nanoparticles was measured in 10 mM KCl at a pH = 7, using the Zetasizer Nano-ZS Zen 3600 (Malvern) with dynamic light scattering (DLS) technology.

Asphaltene Onset Determination

In this study, n-heptane was used to induce asphaltene precipitation. Hence, we define the onset of asphaltene as the minimum volumetric percentage of n-heptane required for the detection of asphaltene aggregates. The onsets of the four crude oils studied were determined based on the indirect method established by Tavakkoli et al.[29] This method was chosen because it has shown to be more sensitive compared to other direct detection methods such as microscopy or refractive index measurement, which limit the aggregate size detection to a minimum of 500 nm. In the indirect method, briefly, samples with different ratios (0-90%) of n-heptane to crude oil were prepared. After aging for 1 hour, the samples were centrifuged for 15 minutes at 10,000 rpm to remove all asphaltene particles larger than 100 nm. The supernatant liquid was then collected and diluted with toluene, and the absorbance of the resulting solution was measured at the wavelength of 1000nm using a Genesys 10S UV-Vis Spectrophotometer (Thermo Scientific). After correction of the dilution effect, the absorbance values were plotted against the volume fraction of n-heptane added. The point of sudden deviation from linear behavior in the data points corresponds to the asphaltene onset of that crude oil. By looking at the supernatant liquid, the sensitivity of the indirect method can be as low as aggregate size of 100 nm.

Characterization of Asphaltene Aggregate

The size of the asphaltene aggregates of each crude oil around the onset of asphaltene was measured using the Zetasizer Nano-ZS Zen 3600 (Malvern) with dynamic light scattering (DLS) technology. The crude oil/n-heptane mixture is very opaque; to allow light to

pass through the mixture, each sample was diluted 100x in cyclohexane. Cyclohexane is considered a neutral solvent for asphaltenes, meaning it does not solubilize asphaltenes nor contribute to their aggregation.

The zeta potential of the aggregates was measured using the DelsaMax Pro (Beckman Coulter). The sample was prepared by suspending 50 mg of fractionated asphaltenes in 10 mL of cyclohexane. The mixture was then probe sonicated for 5 minutes and was let equilibrated for 1 hour to let the larger asphaltene aggregates settle. The supernatant with the suspended asphaltenes was then analyzed.

Time-of-Flight Secondary Ion Mass Spectroscopy (ToF-SIMS) Measurement of Asphaltenes

The composition of the asphaltenes with and without the nanoparticle coating was studied using ToF-SIMS. ToF-SIMS measurements were performed using a ToF-SIMS NCS instrument, which combines a ToF-SIMS instrument (ION-TOF GmbH, Münster, Germany) and an in-situ Scanning Probe Microscope (NanoScan, Switzerland) at Shared Equipment Authority from Rice University. Large image has been obtained by stitching collected mappings from a stage area of 35.5 mm x 11.5 mm using 72 by 23 patches. A bunched 30 keV Bi_3^+ ions (with a measured current of 0.25 pA) was used as a primary probe for analysis (scanned area 500 x 500 µm^2 for each patch. with a raster of 128 x 1280 pixels. A charge compensation with an electron flood gun has been applied during the analysis. An adjustment of the charge effects has been operated using the appropriate surface potential and adapted extraction bias depending on the analysis area and the polarity. The cycle time was fixed to 100 µs (corresponding to m/z = 0 - 911 a.m.u. mass range). The primary ion dose density has been limited to 1.10^{22} ions/cm^2 to preserve the analyzed surface.

Microfluidic Experiment

1. Microfluidic Device Fabrication

The microfluidic devices were fabricated using NOA-81 material (Norland Optical Adhesive), a thiolene-based photocurable polymer,[30] according to the previously published procedures by Vavra et al.[31,32] The microfluidic device in this study is a single permeability porous media made up of round posts (Figure 1a), with a porosity of 91.6%. This microfluidic design can highlight asphaltene deposition from the complex fluid flow within the near-wellbore region. The specifications of the microfluidic device are listed in Table 2.

Table 2: Geometrical Parameters of the Porous Microfluidic Device

Porous media's length	1 mm
Porous media's width	0.2 mm
Post's diameter	120 µm
Post's thickness	80 µm
Row distance	280 µm
Column distance	220 µm
Porosity	91.6%
Permeability	20.2 Darcy

2. AA-AMPS-MNPs Coating of Microfluidic Device

A 500 ppm solution of AA-AMPS-MNPs was injected into the microfluidic device using a syringe pump (KD Scientific) at a flow rate of 10 µm/min for the duration of 20 hours. The device was then gently dried off using gentle nitrogen flow to remove all residual water before the asphaltene deposition experiments. The nanoparticles strongly adsorb onto the substrate surface due to the chemical interaction between the sulfonate groups ($R\text{-}SO_3^-$) from the grafted copolymers on the nanoparticle surface and the active groups exposed on the substrate surface, consisting of different hydroxyl groups (Si-OH, Al-OH) and carboxyl group (C-OOH). This substrate was chosen because it resembles the sandstone reservoir, whose rocks have similar surface active groups. This indicates good nanoparticle adsorption for reservoir application.

3. Asphaltene Deposition in Microfluidics

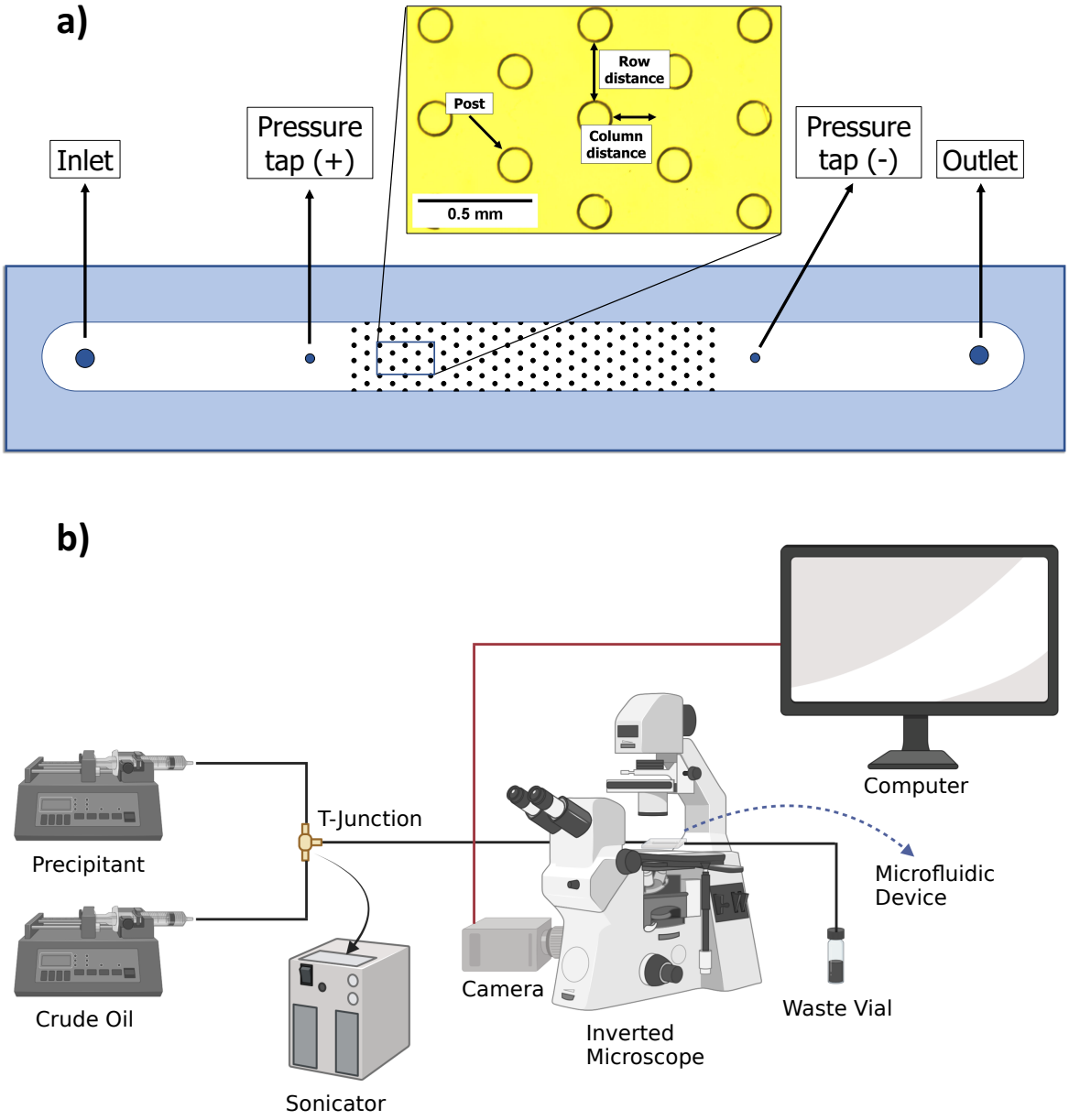

Figure 1: a) Illustration of the porous media microfluidic device, and b) Experimental setup for the asphaltene deposition in microfluidics.

Asphaltene deposition experiments in microfluidics were conducted at room temperature and atmospheric pressure following the experimental setup illustrated in Figure 1b. Crude oil and precipitant (n-heptane) were co-injected at a predetermined ratio at a total flowrate of 60 µm/min using a dual-rate syringe pump (KD Scientific) through a T-junction (IDEX, MicroTee Assembly PEEK, 1/16 in.) into the inlet of the microfluidic device. The T-junction was submersed in an ultra-sonic bath (Branson B1510R-DTH Ultrasonic Cleaner) to enhance the mixing of fluids. A pressure transducer (Valedyne P-61) was connected to the device to measure the pressure drop across the porous media during the experiment, with pressure being recorded every second. The microfluidic device was staged under an inverted microscope (Olympus IX 81) connected to a CCD camera (IMPERX IGV-B1621), where all in-situ processes were monitored and recorded. The effluent from the outlet of the microfluidic device was collected in a waste vial.

Results and Discussion

Nanoparticle Characterization

The hydrodynamic diameters of the three types of MNPs are shown in Table 3. While the hydrodynamic diameters of MNPs and NH_2-MNPs are similar, averaging between 120-140 nm, the average diameter of AA-AMPS-MNPs increases to around 240 nm. The large increase in the diameter of the nanoparticles after the copolymer functionalization has also been observed previously by Xue et al,[12] and was associated with the bridging of NH_2-MNPs with the carboxylates on the AA-AMPS copolymers.

The zeta potential of the MNPs were also measured in 10 mM KCl solution at pH = 7. NH_2-MNPs show positive zeta potential at 13.8 mV due to the presence of amine functionalization on the surface. The grafting of negatively-charged AA-AMPS copolymers onto the nanoparticles' surface leads to charge inversion, resulting in the zeta potential of AA-AMPS-MNPs turning negative at -28.4 mV.

Table 3: Hydrodynamic diameter and zeta potential of the three types of MNPs

Types of MNPs	Average hydrodynamic diameter (nm)	Zeta potential (mV)
MNPs	146.4	-23.7
NH_2-MNPs	122.3	13.8
AA-AMPS-MNPs	242.7	-28.4

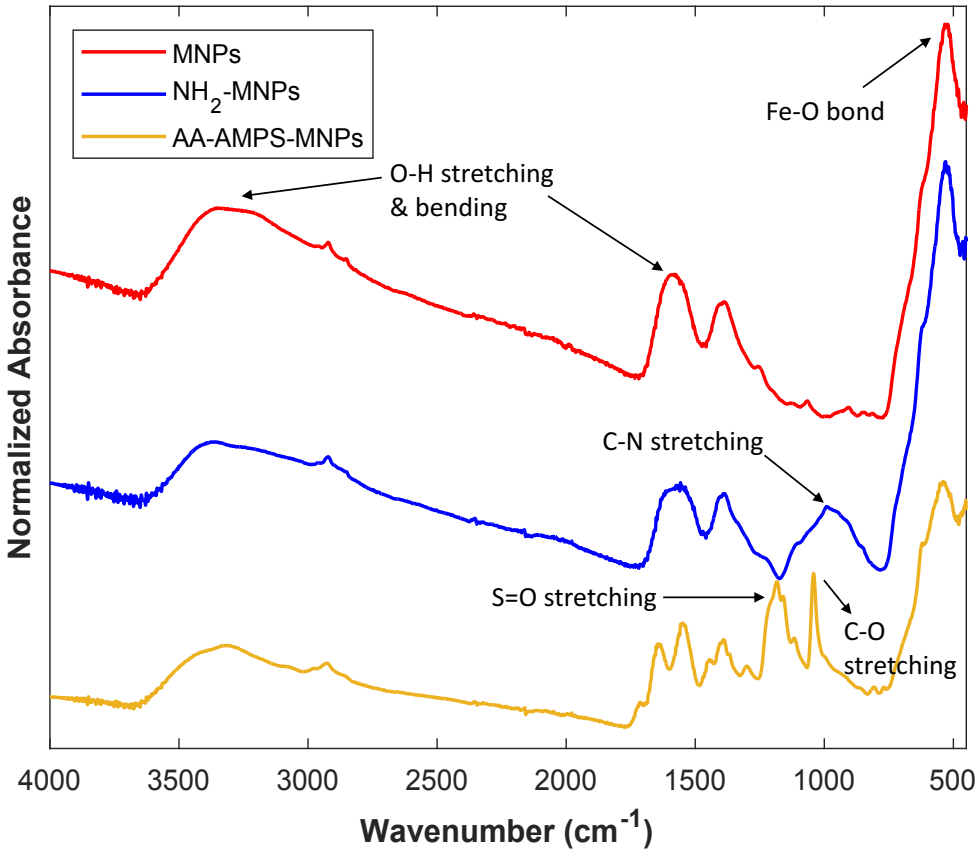

Figure 2: FTIR spectra of MNPs, NH_2-MNPs, and AA-AMPS-MNPs.

Figure 2 shows the FTIR spectra of the MNPs, NH_2-MNPs, and AA-AMPS-MNPs. The three spectra share common peaks at 535 cm^{-1}, 1600 cm^{-1}, and 3360 cm^{-1}. The intense peak observed at 535 cm^{-1} is attributed to the stretching vibration mode associated with the Fe - O bond characteristic of the Fe_3O_4 nanoparticles.[33,34] The broad peaks observed at 1600 cm^{-1} and 3360 cm^{-1} are associated with the O - H bond stretching and bending vibration of water, respectively. This is due to the fact that the nanoparticles are synthesized in aqueous solution, which leads to hydroxyl groups (-OH) binding onto the nanoparticles' surface.

On the spectra of NH_2-MNPs, a broad peak was observed at the wavenumber of 980 cm^{-1}. This peak is associated with the C - N stretching, indicating the presence of amine groups on the surface of the Fe_3O_4 nanoparticles[35,36]

Several additional peaks were observed on the FTIR spectrum of AA-AMPS-MNPs. The peak at the wavenumber of 1187 cm^{-1} is associated with the C - O stretching on a secondary alcohol. Another peak at 1381 cm^{-1} is associated with the S = O stretching on a sulfonate. These peaks are characteristic of the AA-AMPS copolymer, indicating the successful functionalization of MNPs.

Identifying the Onset of Asphaltene

Following the indirect method, the asphaltene onsets of the four crude oils are identified as the points where the absorbance of the crude oil/n-heptane mixture deviates from linearity with increasing n-heptane volume percentage.[29] While the onsets of crudes A, B, and C can be distinctly identified, crude D behaves differently from the rest, such that no significant deviation from linearity could be defined (Figure 3). We hypothesize that at ambient pressure, asphaltenes in crude D are thermodynamically unstable and can aggregate even without the addition of n-heptane. Table 4 summarizes the asphaltene onset as well as the microfluidic operating condition of each crude oil. It is important to note that the operating conditions were set at slightly higher n-heptane volume percentages compared to the asphaltene onsets. This is to ensure that sufficient asphaltene precipitation would be

observed and quantified during the microfluidic experiments.

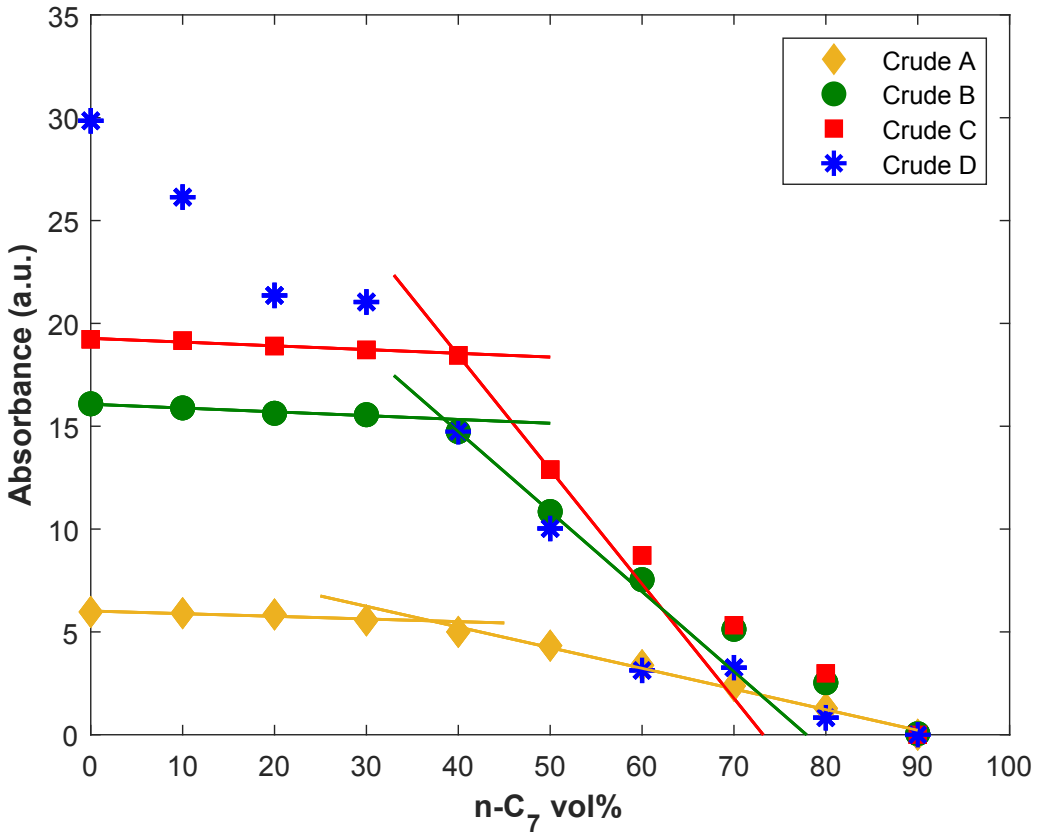

Figure 3: Results of the indirect method to identify the asphaltene onsets of the four crude oils.

Asphaltene Deposition in Microfluidics

Figure 4 shows the asphaltene deposition profiles inside the non-modified microfluidic device of the four crude oils after 60 minutes of deposition. It is important to note that due to the microscope's limited field of view, images can only be captured from one area of the microfluidic device. Thus, pressure drop was measured in complement of the microfluidic imaging to capture the overall change in permeability of the porous media. All microfluidic data images in this study were taken from the same area pf the porous media to ensure consistent analysis.

Table 4: Asphaltene onsets and microfluidic operating conditions of the four crude oils

Crude Oil	Asphaltene Onset (n-heptane vol%)	Microfluidic Operating Condition (n-heptane vol%)
Crude A	37	45
Crude B	39	50
Crude C	40	50
Crude D	-	45

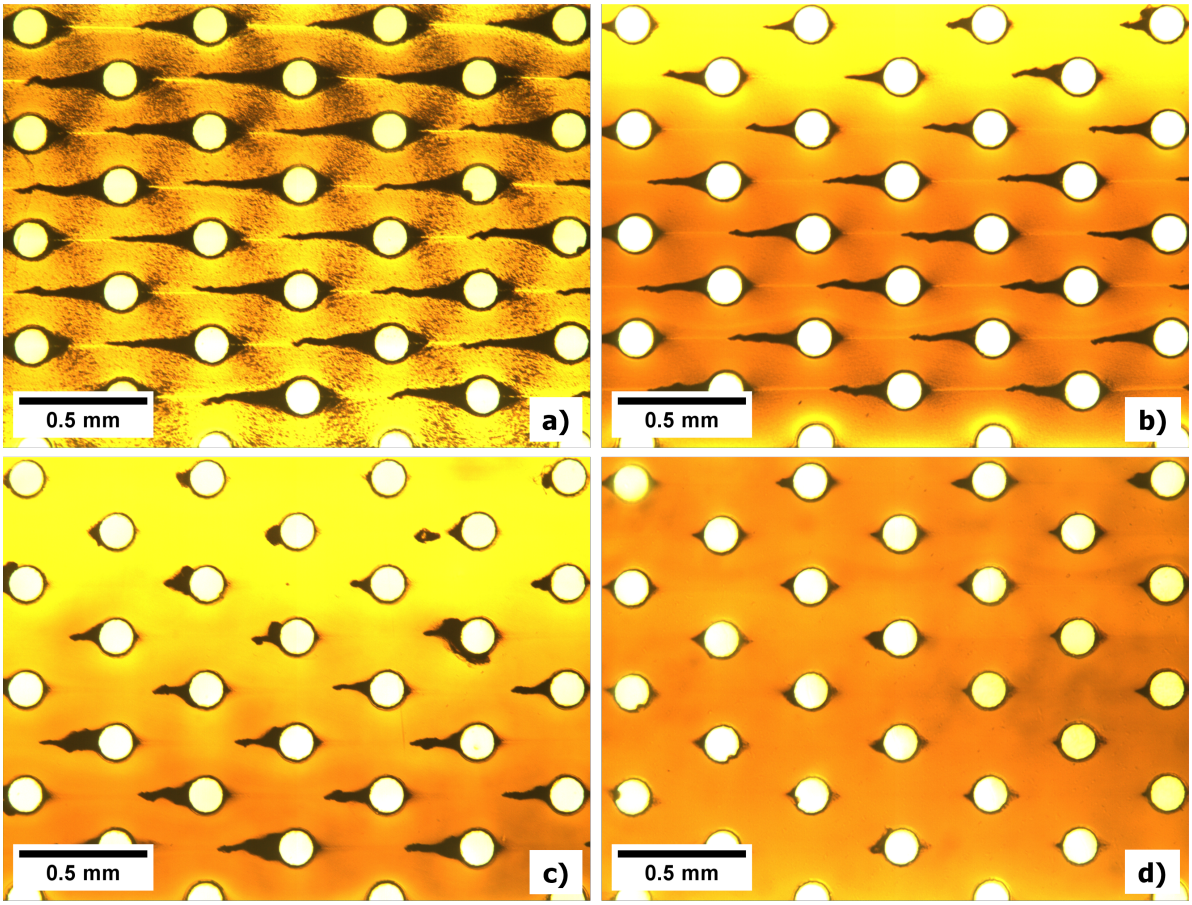

Figure 4: Asphaltene deposition profiles after 60 minutes of a) Crude A, b) Crude B, c) Crude C, and d) Crude D. Fluid flows from left to right.

It can be shown that despite the high asphaltene contents, crude C and crude D show significantly less deposition than crude A and crude B. This phenomenon has previously been observed, such that high asphaltene content in an oil is not necessarily associated with the high risk of asphaltene precipitation and deposition.[24] From the microfluidic imaging data, it can be seen that the asphaltene deposits on the post from crudes A and B are very uniform and well-stacked compared to crudes C and D, where the deposits' structures vary significantly across the posts. In the case of crude A, asphaltene aggregates not only deposit on the posts making up the porous media but also deposit on the upper and lower surfaces of the microfluidic device. This phenomenon was not observed in the other crude oils. This demonstrated that asphaltenes from different sources can have very different adsorption tendencies to the same substrate.

Table 5: Average asphaltene aggregate size at microfluidic operating condition

Crude Oil	Average Aggregate Size (µm)	Péclet Number
Crude A	1.67	$1.5\text{x}10^7$
Crude B	3.12	$8.7\text{x}10^7$
Crude C	4.79	$2.9\text{x}10^8$
Crude D	4.17	$3.6\text{x}10^8$

During the microfluidic experiments, it was observed that the asphaltene aggregates from crude A were much finer in size compared to those from crudes C and D. This observation was confirmed by the size distribution of asphaltene aggregates from DLS measurements. Table 5 summarizes the average aggregate size of each crude oil, showing that the aggregate sizes from crudes C and D are approximately 3 times larger than those from crude A. The Péclet number (Pe) was calculated for each case (Table 5), which is the ratio of the advection rate to the diffusion rate. The equations used to calculate the Péclet number are shown below

$$Pe = \frac{2uR_p}{D_{BM}} \tag{1}$$

$$D_{BM} = \frac{k_B T}{6\pi\mu R_p} \tag{2}$$

where R_p is the average radius of the aggregate, D_{BM} is the Brownian diffusivity, assuming a spherical aggregate, u is the superficial velocity of the flow, μ is the dynamic viscosity of the mixture, k_B is the Boltzman constant, and T is the temperature.

It can be shown that crudes A and B have Péclet numbers roughly an order of magnitude lower than those of crude C and D. The two key factors making up the differences between the two cases are the asphaltene aggregates size and the viscosity of each mixture, such that the Péclet number decreases with decreasing aggregate size, and increases with increasing viscosity. With smaller aggregate sizes as observed in crudes A and B, the aggregate diffusivity increases, leading to higher aggregate deposition on the posts. Secondly, the viscosities of crudes C and D are significantly higher than those of crudes A and B. This leads to higher shear forces exerted by the flow, which can easily remove the inefficient packing form by large aggregates. Lin et al. suggested that there exists a threshold of the Péclet number at which asphaltene aggregates become stable and are no longer easily removed by the shear flow.[10] This is dependent on the intermolecular interactions between the asphaltene aggregates, which are tied to the nature of the crude oils. This is, however, beyond the scope of this study and will not be discussed.

Effectiveness of MNP-coating in Asphaltene Mitigation on Different Crude Oils

1. Crude A

Figure 5 shows the asphaltene deposition profiles from crude A after 60 minutes in the control (a) and the nanoparticle (NP)-coated (b) microfluidic devices. As noted previously, the asphaltene deposits were well-packed and uniformly distributed in both cases. The NP-coated microfluidic device shows less severe asphaltene deposition compared to the control case. To accurately quantify the amount of asphaltene deposition across the device, the pressure drop measurements of the two cases were recorded. In Figure 5c, the pressure drop plots are calculated based on the moving average of the pressure drop measurements and are

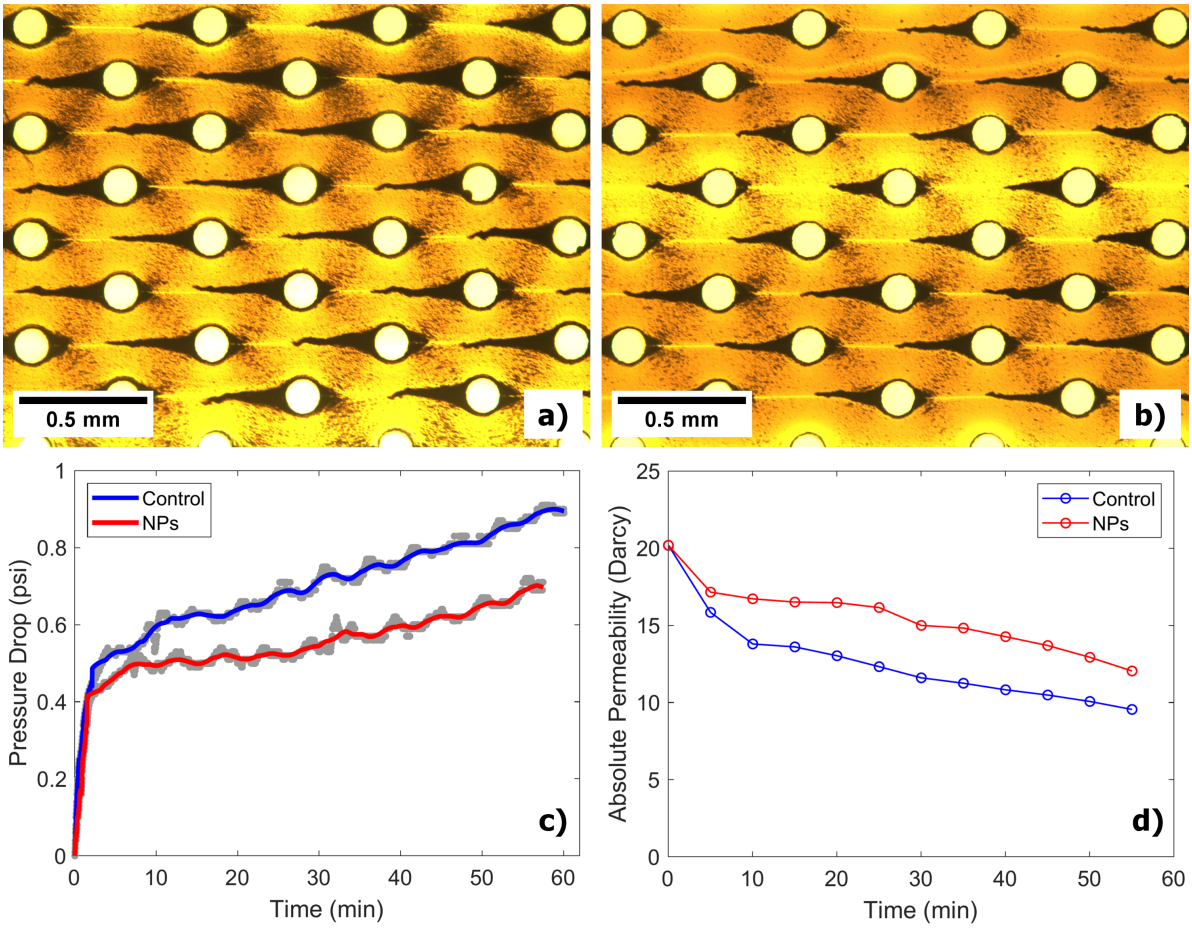

Figure 5: Asphaltene deposition profile of crude A in a) control case and b) NP-coated case. c) shows the pressure drop measurements of the two cases, and d) shows the change in absolute permeability as a result of asphaltene deposition.

used to eliminate the noise typically observed in pressure drop measurements.

In a typical microfluidic experiment, the pressure drop increases quickly in the first minute of the experiment as the fluid enters the porous media, establishing a pressure gradient as a result of the fluid flow. The more gradual increase in pressure drop after this is associated with the reduction in the permeability of the device due to asphaltene deposition. The change in permeability was calculated from Darcy's equation:

$$q = \frac{kA\Delta P}{\mu L} \tag{3}$$

where q is the total flow rate, k is the permeability of the porous media, A is the cross-sectional area, ΔP is the pressure drop, μ is the viscosity of the fluid, and L is the length of the porous media. Figure 5d shows the absolute permeabilities of the two cases, where at the end of the experiment, the permeability of the control device was 9.4 Darcy, and that of the NP-coated device was 12.1 Darcy. The original permeability of the device was 20.2 Darcy. From this, it can be concluded that the nanoparticle coating has a positive effect on asphaltene inhibition in crude A, showing a 25% improvement in permeability reduction.

2. Crude B

Figure 6 shows the asphaltene deposition profiles from crude B after 60 minutes in the control (a) and the NP-coated (b) microfluidic devices. It can be shown that the tails of the deposits in the NP-coated case were shorter than those in the control case. The pressure drop measurements show an even more pronounced effect of the nanoparticle-coating, where the pressure drop in the control case increased significantly over the course of the experiment, while that of the NP-coated case changed minimally (Figure 6c). The final permeabilities of the control and the NP-coated devices were 7.9 Darcy and 14.1 Darcy, respectively. Nanoparticle-coating is particularly effective in inhibiting asphaltene deposition in crude oil B, showing 51% less permeability reduction.

3. Crude C

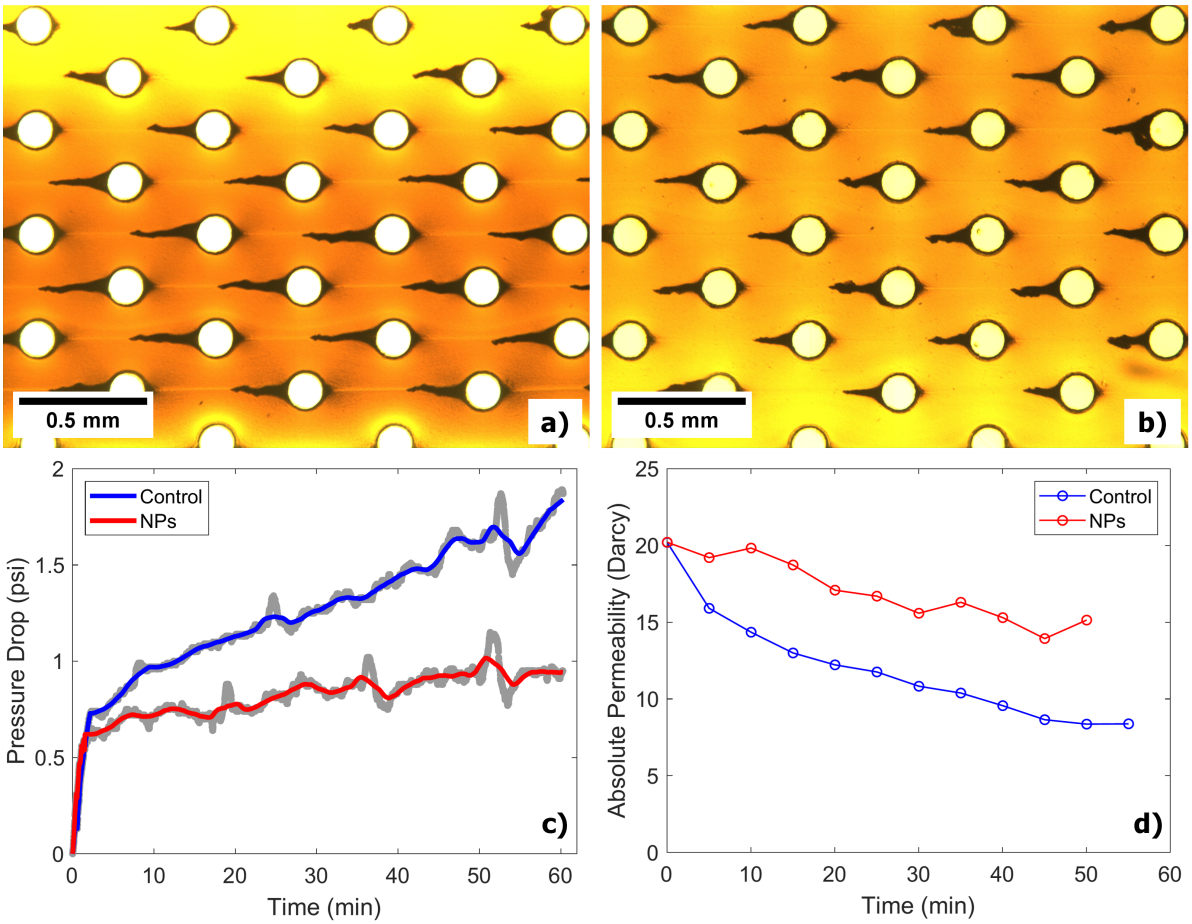

Figure 6: Asphaltene deposition profile of crude B in a) control case and b) NP-coated case. c) shows the pressure drop measurements of the two cases, and d) shows the change in absolute permeability as a result of asphaltene deposition.

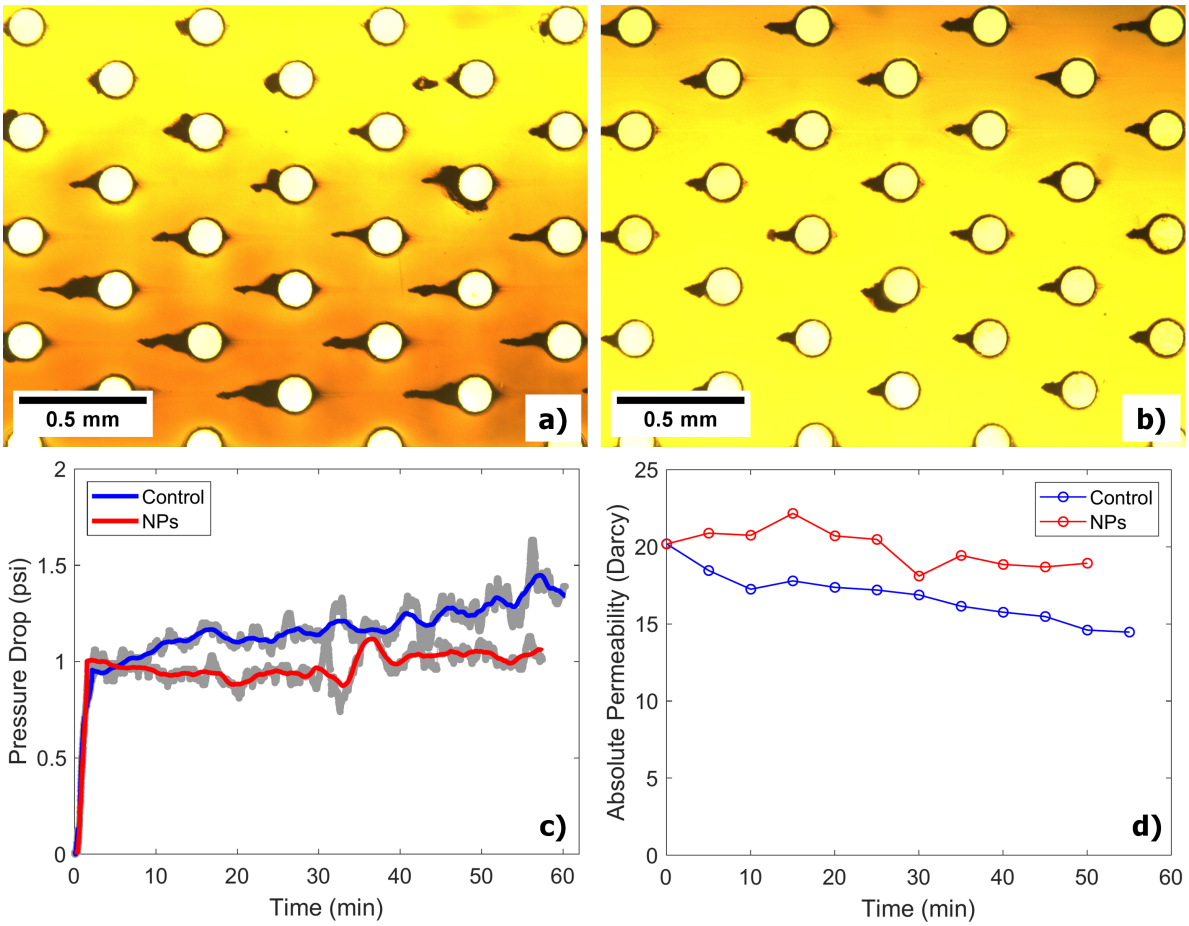

Figure 7: Asphaltene deposition profile of crude C in a) control case and b) NP-coated case. c) shows the pressure drop measurements of the two cases, and d) shows the change in absolute permeability as a result of asphaltene deposition.

The asphaltene deposition profiles in the microfluidic porous media were shown in Figure 7 for the control case (a), and the NP-coated case (b). The asphaltene deposits observed in this crude oil were non-uniform across the porous media due to the larger aggregate sizes leading to inefficient packing. The microfluidic image shows many large asphaltene deposits in the control device, indicating that the large aggregates that are stable enough to form a deposit would cause significant permeability reduction. These large deposits were not observed in the NP-coated case, indicating that the NP-coated surface considerably reduces the tendency of these large aggregates to absorb and deposit. The pressure drop measurement shows that there was a very insignificant change in the permeability in the NP-coated microfluidic device, with the absolute permeabilities of the control and the NP-coated case being 14.0 Darcy and 18.7 Darcy, respectively. For crude C, the nanoparticle coating shows roughly 75% improvement in asphaltene deposition inhibition.

4. Crude D

Crude D did not show severe asphaltene deposition, despite having the highest asphaltene content at around 18 wt % according to the SARA analysis. During the microfluidic experiments, large asphaltene aggregates were observed flowing through the porous media but not frequently adsorb onto the posts. Virtually no asphaltene deposit was observed in the NP-coated case, except for the upper edge of the device, which shows some asphaltene deposition. This can be explained by the uneven coating of the nanoparticles on the device, such that the edge of the device did not get good nanoparticle coverage, leading to more asphaltene deposition. The pressure drop measurements as well as the absolute permeabilities in each case are shown in Figure 8c&d. Due to insignificant asphaltene deposition, the difference in the final permeability of the two devices is not considerable. The absolute permeabilities of the control and the NP-coated case at the end of the experiment are 14.4 and 16.2, respectively. The nanoparticle coating shows a 31% improvement in permeability reduction by asphaltene deposition.

5. Comparison of Permeability Improvement by the Use of AA-AMPS-MNP

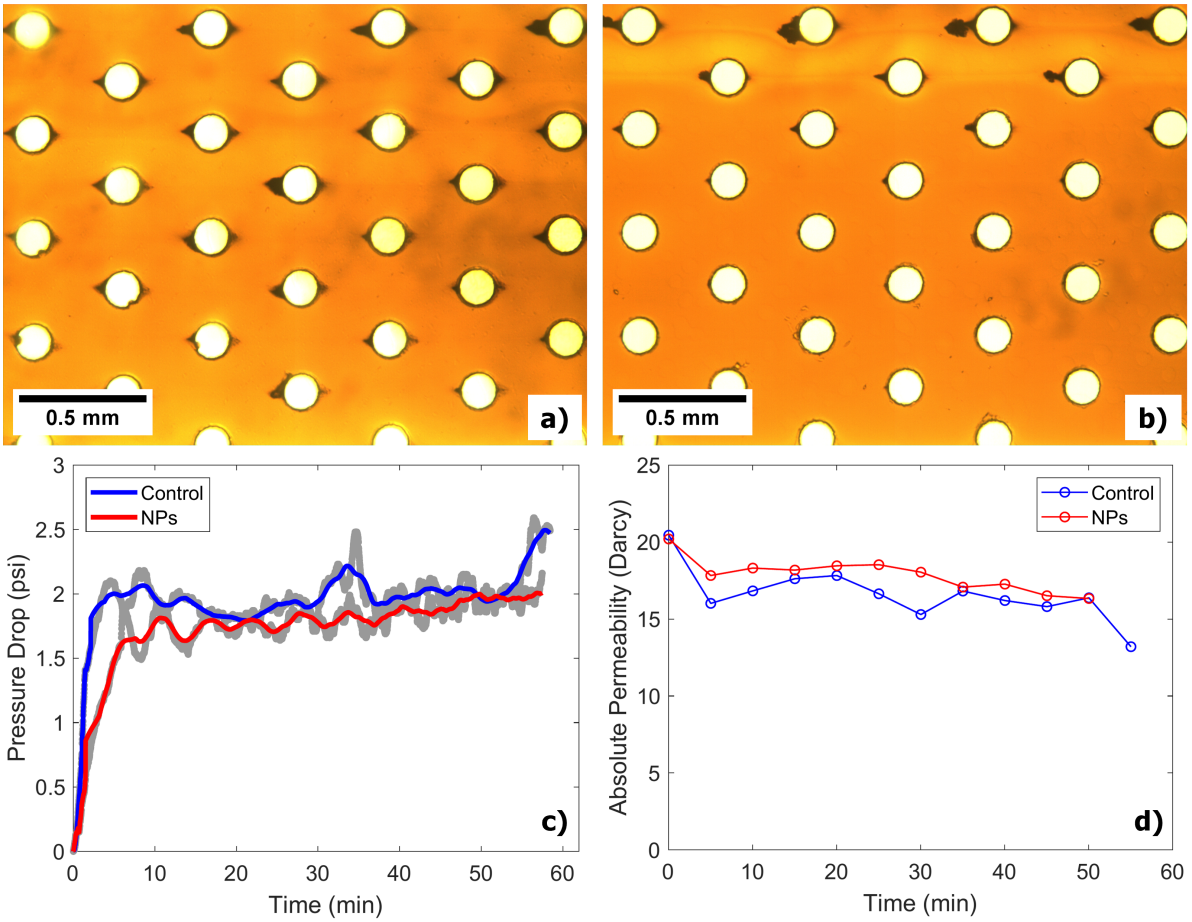

Figure 8: Asphaltene deposition profile of crude D in a) control case and b) NP-coated case. c) shows the pressure drop measurements of the two cases, and d) shows the change in absolute permeability as a result of asphaltene deposition.

coating

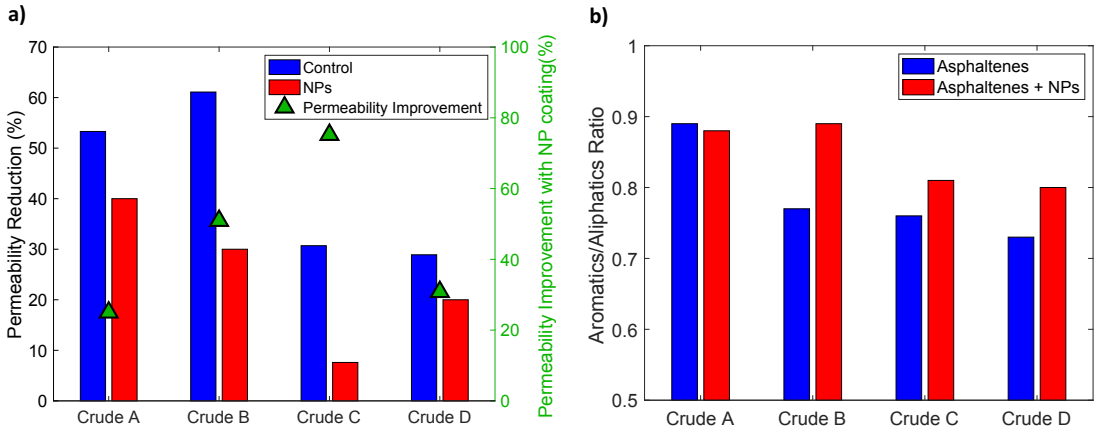

Figure 9: a) Summary of permeability reduction from asphaltene in each crude oil and the effectiveness of NP coating in permeability improvement, and b) Change in aromatics/aliphatics ratios of asphaltenes by NP coating.

Figure 9a summarizes the permeability reduction in both the control and NP-coated cases of each of the crude oils as well as the effectiveness of the nanoparticle coating on improving permeability reduction. Overall, our nanoparticle coating shows effectiveness with all crude oils in improving permeability reduction through asphaltene inhibition, with improvement percentages ranging from 25-75%. Different crude oils were shown to respond differently to the nanoparticle coating. While the effects of asphaltene aggregate size and shear forces were discussed previously, the asphaltene structures as well as the intermolecular interaction between aggregates and between the aggregates and the substrate surface also play an important role in the effectiveness of the mitigation methods.

The presence of the negatively-charged, polyelectrolyte, long-chained AA-AMPS copolymer introduces a layer of steric repulsion to the asphaltene aggregate, but the charge-induced electrostatic repulsion is the most crucial mechanism in preventing asphaltene aggregate from depositing. Table 6 summarizes the zeta potential of asphaltenes from the crude oils in cyclohexane. As shown, in general, asphaltenes exhibit negative zeta potential in nonpolar solvent. However, the magnitude of the potential is not necessarily correlated to the effectiveness of the nanoparticle coating on each crude oil. More specifically, crude A shows the most

negative zeta potential at -9.97 mV, but also shows the least improvement in permeability with nanoparticle coating (25%). On the other hand, crude C shows less negative potential (-1.67 mV) but is the most responsive to the nanoparticle coating. This demonstrates that even though charge-induced electrostatic repulsion plays a crucial role in reducing asphaltene deposition through the negatively-charged polymer-functionalized nanoparticle coating, the interactions between specific functional groups on each type of asphaltenes with the functional groups on the polymers can dictate the overall effectiveness of the nanoparticle coating and can be very complex. Lin et al. showed that island- and archipelago-type asphaltenes exhibit very different deposition behaviors, with the archipelago-type asphaltenes having softer deposit formation and lower deposition tendency.[37] Further analysis of the composition of the subfractions of each type of asphaltenes can give better insights into the role of asphaltene subfractions on the effectiveness of the nanoparticle coating.

Table 6: Zeta potential of asphaltenes from different crude oils in cyclohexane.

Crude Oil	Zeta Potential (mV)
Crude A	-9.97
Crude B	-2.33
Crude C	-1.67
Crude D	-1.26

Many studies have shown that surface chemistry and electrostatic repulsion play an important role in asphaltene adsorption and deposition.[38–41] However, due to the complexity of the mineral composition as well as the surrounding fluid environment in each reservoir, it is hard to predict and control the extent of asphaltene deposition in each case. The use of nanoparticle coating introduces an approach to controlling the surface charge of the substrate, thus indirectly inhibiting asphaltene adsorption and deposition from the surface. With a similar approach, different kinds of copolymer can be considered for grafting to show higher effectiveness in different crude oil systems.

Overall, it was shown that the coating of nanoparticles onto the substrate surface does not completely inhibit asphaltene deposition; in fact, it limits the asphaltene depositing

tendency and lengthens the time required for asphaltenes to cause clogging issues. Therefore, exploring the differences in the fractions of asphaltenes that were removed and the fractions of asphaltenes that were retained can allow interesting insight into the more "stubborn" asphaltene fractions. ToF-SIMS was used to measure the aromatics and aliphatics contents of the asphaltenes of each crude oil and the asphaltenes that were retained on the NP-coated surface (see Supplemental Information). Figure 9b shows that three out of four retained asphaltenes samples exhibited an increase in the aromatics/aliphatics ratio compared to the original asphaltenes. This demonstrates that the nanoparticle coating is more effective in preventing the aliphatic-rich asphaltene fractions from depositing compared to the aromatic-rich fractions. Previous study has shown that the aromatic rings tend to aggregate due to π-stacking, while the long aliphatic chains tend to prevent this aggregation.[42] It can be concluded that the aromatic-rich asphaltene fractions are the more problematic fractions that can aggregate and deposit even in the presence of the nanoparticle coating. This insight can provide more guidance into the design of different polymers that can more effectively target these problematic fractions of asphaltenes.

Conclusion

In conclusion, this study introduced the synthesis and characterization of AA-AMPS-functionalized magnetic nanoparticles that are effective in preventing asphaltene deposition. By taking advantage of the steric and electrostatic repulsions exerted by the long-chained, polyelectrolytes copolymers on the surface of the nanoparticles, the use of nanoparticle coating can significantly prevent asphaltene adsorption and deposition on the substrate surface, showing up to 75% improvement in permeability reduction. The nanoparticles are also relatively inexpensive to synthesize, making this a viable technique to combat asphaltene problems in the reservoir. Furthermore, with the help of microfluidic technology, this study allowed for a closer look into the asphaltene deposition tendency of different crude oils. The

stability of the aggregate deposits is dependent on the aggregate sizes and the viscosity of the fluid mixture, as well as the intermolecular interactions that are governed by the specific functional groups and chemical compositions that make up the asphaltene molecule.

Supporting Information

Summary tables showing ToF-SIMS data on the aliphatic and aromatic compositions of all asphaltenes.

Acknowledgement

The authors acknowledge the National Science Foundation Award TI-2141112 and Deepstar Consortium for the financial support for this project. ToF-SIMS analysis was carried out with the support provided by the National Science Foundation CBET-1626418. The bio-screening plate containing 10 microns-deep microwells was manufactured by Carlos Gramajo on a glass slide using a Universal X-660 Laser Cutter Platform. This work was conducted in part using resources from the Shared Equipment Authority at Rice University.

References

(1) Tavakkoli, M.; Panuganti, S. R.; Taghikhani, V.; Pishvaie, M. R.; Chapman, W. G. Understanding the Polydisperse Behavior of Asphaltenes during Precipitation. *Fuel* **2014**, *117*, 206–217.

(2) Vargas, F. M., Tavakkoli, M., Eds. *Asphaltene Deposition: Fundamentals, Prediction, Prevention, and Remediation*; CRC Press, Boca Raton, FL, 2018; Chapter 1: Introduction.

(3) Kokal, S. L.; Sayegh, S. G. Asphaltenes: The Cholesterol Of Petroleum. Middle East Oil Show. Bahrain, 1995.

(4) Chaisoontornyotin, W.; Haji-Akbari, N.; Fogler, H. S.; Hoepfner, M. P. Combined Asphaltene Aggregation and Deposition Investigation. *Energy Fuels* **2016**, *30*, 1979–1986.

(5) Chaisoontornyotin, W.; Bingham, A. W.; Hoepfner, M. P. Reversibility of Asphaltene Precipitation Using Temperature-Induced Aggregation. *Energy Fuels* **2017**, *31*, 3392–3398.

(6) Gruesbeck, C.; Collins, R. E. Entrainment and Deposition of Fine Particles in Porous Media. *Soc. Pet. Eng. J.* **1982**, *22*, 847–856.

(7) Wang, S.; Civan, F. Productivity Decline of Vertical and Horizontal Wells by Asphaltene Deposition in Petroleum Reservoirs. SPE International Symposium on Oilfield Chemistry. Houston, Texas, 2001.

(8) Ahmadbaygi, A.; Bayati, B.; Mansouri, M.; Rezaei, H.; Riazi, M. Chemical Study of Asphaltene Inhibitors Effects on Asphaltene Precipitation of an Iranian Oil field. *Oil Gas Sci. Technol. – Rev. IFP Energies nouvelles* **2020**, *75*, 6.

(9) Lun, Z.; Liu, Y.; Zhang, Q.; Liu, M.; Liu, J.; Yang, P. Study on Inhibition Behaviors of Asphaltene Inhibitor to Asphaltene Aggregations. *J. Dispers. Sci. Technol.* **2021**, 1–9.

(10) Lin, Y.-J.; He, P.; Tavakkoli, M.; Mathew, N. T.; Fatt, Y. Y.; Chai, J. C.; Goharzadeh, A.; Vargas, F. M.; Biswal, S. L. Characterizing Asphaltene Deposition in the Presence of Chemical Dispersants in Porous Media Micromodels. *Energy Fuels* **2017**, *31*, 11660–11668.

(11) Kahs, T.; Raj, G.; Whelan, J.; Larkin, E.; Commins, P.; Punnapala, S.; Odeh, N.; Abdallah, D.; Naumov, P. Evaluation of the Effectiveness of Inhibitors for Middle

Eastern Asphaltenes by Quartz Crystal Microbalance with Dissipation. *Energy Fuels* **2022**, *36*, 8786–8798.

(12) Xue, Z.; Foster, E.; Wang, Y.; Nayak, S.; Cheng, V.; Ngo, V. W.; Pennell, K. D.; Bielawski, C. W.; Johnston, K. P. Effect of Grafted Copolymer Composition on Iron Oxide Nanoparticle Stability and Transport in Porous Media at High Salinity. *Energy Fuels* **2014**, *28*, 3655–3665.

(13) Pagán Pagán, N. M.; Zhang, Z.; Nguyen, T. V.; Marciel, A. B.; Biswal, S. L. Physicochemical Characterization of Asphaltenes Using Microfluidic Analysis. *Chem. Rev.* **2022**, *122*, 7205–7235.

(14) Lin, Y.-J.; Barman, S.; He, P.; Zhang, Z.; Christopher, G. F.; Biswal, S. L. Combined Interfacial Shear Rheology and Microstructure Visualization of Asphaltenes at Air-Water and Oil-Water Interfaces. *J. Rheol.* **2018**, *62*, 1–10.

(15) Doryani, H.; Malayeri, M.; Riazi, M. Visualization of Asphaltene Precipitation and Deposition in a Uniformly Patterned Glass Micromodel. *Fuel* **2016**, *182*, 613–622.

(16) Hu, C.; Hartman, R. L. High-Throughput Packed-Bed Microreactors with In-Line Analytics for the Discovery of Asphaltene Deposition Mechanisms. *AIChE J.* **2014**, *60*, 3534–3546.

(17) Zhuang, Y.; Goharzadeh, A.; Lin, Y. J.; Yap, Y. F.; Chai, J. C.; Mathew, N.; Vargas, F.; Biswal, S. L. Experimental study of asphaltene Deposition in Transparent Microchannels Using the Light Absorption Method. *J. Dispers. Sci. Technol.* **2018**, *39*, 744–753.

(18) Sieben, V. J.; Tharanivasan, A. K.; Ratulowski, J.; Mostowfi, F. Asphaltenes Yield Curve Measurements on a Microfluidic Platform. *Lab Chip* **2015**, *15*, 4062–4074.

(19) Haider, O. M.; Ma, J.; Grzesiak, K. A.; Walker, L. M. Advantages of a Millifluidic Approach to the Characterization of Long-Time Solvency Effects on Bulk Asphaltene Precipitation. *Energy Fuels* **2023**, *37*, 2791–2798.

(20) Anisimov, M. A.; Ganeeva, Y. M.; Gorodetskii, E. E.; Deshabo, V. A.; Kosov, V. I.; Kuryakov, V. N.; Yudin, D. I.; Yudin, I. K. Effects of Resins on Aggregation and Stability of Asphaltenes. *Energy Fuels* **2014**, *28*, 6200–6209.

(21) Park, S. J.; Escobedo, J.; Mansoori, G. A. *Developments in Petroleum Science*; Elsevier, Amsterdam, Netherlands, 1994; Chapter 8: Asphaltene and Other Heavy Organic Depositions, pp 179–205.

(22) Leontaritis, K. J.; Ali Mansoori, G. Asphaltene Deposition: a Survey of Field Experiences and Research Approaches. *J. Pet. Sci. Eng.* **1988**, *1*, 229–239.

(23) Ma, J.; Haider, O. M.; Chang, C.-C.; Grzesiak, K. A.; Squires, T. M.; Walker, L. M. Solvent Quality and Aggregation State of Asphaltenes on Interfacial Mechanics and Jamming Behavior at the Oil/Water Interface. *Langmuir* **2023**,

(24) Pedersen, K. S.; Christensen, P. L.; Shaikh, J. A. *Phase Behavior of Petroleum Reservoir Fluids*, 2nd ed.; CRC Press, Boca Raton, FL, 2015.

(25) Yoon, K. Y.; Li, Z.; Neilson, B. M.; Lee, W.; Huh, C.; Bryant, S. L.; Bielawski, C. W.; Johnston, K. P. Effect of Adsorbed Amphiphilic Copolymers on the Interfacial Activity of Superparamagnetic Nanoclusters and the Emulsification of Oil in Water. *Macromolecules* **2012**, *45*, 5157–5166.

(26) Prieve, D. C.; Ruckenstein, E. Role of Surface Chemistry in Primary and Secondary Coagulation and Heterocoagulation. *J. Colloid Interface Sci.* **1980**, *73*, 539–555.

(27) Hogg, R.; Healy, T. W.; Fuerstenau, D. W. Mutual Coagulation of Colloidal Dispersions. *Trans. Faraday Soc.* **1966**, *62*, 1638.

(28) Wang, Q.; Puerto, M. C.; Warudkar, S.; Buehler, J.; Biswal, S. L. Recyclable Amine-Functionalized Magnetic Nanoparticles for Efficient Demulsification of Crude Oil-in-Water Emulsions. *Environ. Sci.: Water Res. Technol.* **2018**, *4*, 1553–1563.

(29) Tavakkoli, M.; Grimes, M. R.; Liu, X.; Garcia, C. K.; Correa, S. C.; Cox, Q. J.; Vargas, F. M. Indirect Method: A Novel Technique for Experimental Determination of Asphaltene Precipitation. *Energy Fuels* **2015**, *29*, 2890–2900.

(30) Masouminia, M.; Dalnoki-Veress, K.; de Lannoy, C.-F.; Zhao, B. Wettability Alteration of a Thiolene-Based Polymer (NOA81): Surface Characterization and Fabrication Techniques. *Langmuir* **2023**, *39*, 2529–2536.

(31) Vavra, E. D.; Zeng, Y.; Xiao, S.; Hirasaki, G. J.; Biswal, S. L. Microfluidic Devices for Characterizing Pore-scale Event Processes in Porous Media for Oil Recovery Applications. *J. Vis. Exp.* **2018**, 56592.

(32) Bartolo, D.; Degré, G.; Nghe, P.; Studer, V. Microfluidic Stickers. *Lab Chip* **2008**, *8*, 274–279.

(33) Yusoff, A. H. M.; Salimi, M. N.; Jamlos, M. F. Synthesis and Characterization of Biocompatible Fe_3O_4 Nanoparticles at Different pH. Internation Conference on Advanced Material Engineering and Technology. Kaohsiung City, Taiwan, 2017.

(34) Nalbandian, L.; Patrikiadou, E.; Zaspalis, V.; Patrikidou, A.; Hatzidaki, E.; N. Papandreou, C. Magnetic Nanoparticles in Medical Diagnostic Applications: Synthesis, Characterization and Proteins Conjugation. *Curr. Nanosci.* **2016**, *12*, 455–468.

(35) Karade, V. C.; Sharma, A.; Dhavale, R. P.; Dhavale, R. P.; Shingte, S. R.; Patil, P. S.; Kim, J. H.; Zahn, D. R. T.; Chougale, A. D.; Salvan, G.; Patil, P. B. APTES Monolayer Coverage on Self-Assembled Magnetic Nanospheres for Controlled Release of Anticancer Drug Nintedanib. *Sci. Rep.* **2021**, *11*, 5674.

(36) Majoul, N.; Aouida, S.; Bessaïs, B. Progress of porous silicon APTES-functionalization by FTIR investigations. *Appl. Surf. Sci.* **2015**, *331*, 388–391.

(37) Lin, Y.-J.; Cao, T.; Chacón-Patiño, M. L.; Rowland, S. M.; Rodgers, R. P.; Yen, A.; Biswal, S. L. Microfluidic Study of the Deposition Dynamics of Asphaltene Subfractions Enriched with Island and Archipelago Motifs. *Energy Fuels* **2019**, *33*, 1882–1891.

(38) Girard, H.-L.; Bourrianne, P.; Chen, D.; Jaishankar, A.; Vreeland, J. L.; Cohen, R. E.; Varanasi, K. K.; McKinley, G. H. Asphaltene Adsorption on Functionalized Solids. *Langmuir* **2020**, *36*, 3894–3902.

(39) Al-Maamari, R. S. H.; Buckley, J. S. Asphaltene Precipitation and Alteration of Wetting: Can Wettability Change during Oil Production? SPE/DOE Improved Oil Recovery Symposium. Tulsa, Oklahoma, 2000.

(40) Mohammed, I.; Al Shehri, D.; Mahmoud, M.; Kamal, M. S.; Alade, O. S. A Surface Charge Approach to Investigating the Influence of Oil Contacting Clay Minerals on Wettability Alteration. *ACS Omega* **2021**, *6*, 12841–12852.

(41) Mohammed, I.; Al Shehri, D.; Mahmoud, M.; Kamal, M. S.; Alade, O. S. Impact of Iron Minerals in Promoting Wettability Alterations in Reservoir Formations. *ACS Omega* **2021**, *6*, 4022–4033.

(42) Rahmati, M. Effects of Heteroatom and Aliphatic Chains of Asphaltene Molecules on Their Aggregation Properties in Aromatics Solvents: A Molecular Dynamics Simulation Study. *Chem. Phys. Lett.* **2021**, *779*, 138847.

TOC Graphic